Smart Structures and Systems, *Vol. 15, No. 6 (2015) 1601-1623*
DOI: http://dx.doi.org/10.12989/sss.2015.15.6.1601

Nonlinear large deformation dynamic analysis of electroactive polymer actuators

Amir Ali Amiri Moghadam[1], Abbas Kouzani[1], Reza Zamani[2], Kevin Magniez[3] and Akif Kaynak[*1]

[1]*School of Engineering, Deakin University, Geelong, Victoria 3216, Australia*
[2]*School of Information Systems and Technology, EIS, University of Wollongong, NSW 2522, Australia*
[3]*Institute for Frontier Materials, Deakin University, Geelong, Victoria 3216, Australia*

(Received March 24, 2014, Revised July 22, 2014, Accepted July 26, 2014)

Abstract. Electroactive polymers have attracted considerable attention in recent years due to their sensing and actuating properties which make them a material of choice for a wide range of applications including sensors, biomimetic robots, and biomedical micro devices. This paper presents an effective modeling strategy for nonlinear large deformation (small strains and moderate rotations) dynamic analysis of polymer actuators. Considering that the complicated electro-chemo-mechanical dynamics of these actuators is a drawback for their application in functional devices, establishing a mathematical model which can effectively predict the actuator's dynamic behavior can be of paramount importance. To effectively predict the actuator's dynamic behavior, a comprehensive mathematical model is proposed correlating the input voltage and the output bending displacement of polymer actuators. The proposed model, which is based on the rigid finite element (RFE) method, consists of two parts, namely electrical and mechanical models. The former is comprised of a ladder network of discrete resistive-capacitive components similar to the network used to model transmission lines, while the latter describes the actuator as a system of rigid links connected by spring-damping elements (sdes). Both electrical and mechanical components are validated through experimental results.

Keywords: polymer actuators; large deformation dynamic analysis; rigid finite element method

1. Introduction

Electroactive polymers (EAPs) are relatively a new and remarkable class of materials which can be used both as sensors and actuators (Bar-Cohen 2001). Conductive polymers (CP), and ionic metal polymer composites (IPMC) are categorized as electroactive polymeric materials which exhibit interesting sensing and actuating behaviors (Smela 2003). They are among the best candidates for use in solar cells, sensors, and actuators (Otero and Teresa 2001, Wallace *et al*. 2003). Due to their (i) large strains of up to 39%, (ii) bio-compatibility, (iii) micro- and nano-scale manufacturing feasibility and, (iv) relatively low actuation voltages (Madden *et al.* 2004, Jager *et al*. 2000, Smela 2003, Shahinpoor *et al*. 2007, Hara *et al*. 2005, Carpi and Smela 2009) EAPs are candidate materials for the state of the art applications in an array of devices ranging from

*Corresponding author, Associate Professor, E-mail: akaynak@deakin.edu.au

http://www.techno-press.org/?journal=sss&subpage=8 ISSN: 1738-1584 (Print), 1738-1991 (Online)

biomedical appliances through artificial organs to micro-electro-mechanical systems (MEMS).

There are also many reports in the literature about the potential applications of electroactive polymers in different robotic systems. (Chen *et al.* 2010) reported the modeling of a robotic fish propelled by an ionic polymer-metal composite actuator. (Bar-Cohen et al. 1998) presented several EAP driven mechanisms that emulate human hand including a gripper, a manipulator arm, and a surface wiper. (Jager *et al.* 2000) extensively reviewed the current progress of micro actuators based on EAPs, describing the micro fabrication of these actuators plus their possible applications in micro systems. (Amiri Moghadam *et al.* 2011a) proposed the application of adaptive neuro-fuzzy inference systems (ANFIS) in kinematic modeling of a soft micro robot based on conjugated polymer actuators.

Based on different fabrication methods, three different configurations of the actuators can be obtained, namely (i) linear extenders, (ii) bilayer benders, and (iii) trilayer benders (Della et al. 1997, Smela *et al.* 1995, Kaneto *et al.* 1995). The main process which is responsible for volumetric change and the resulting actuation ability of the conjugated polymer actuators is reduction/oxidation (RedOx). By applying a voltage to the actuator, the electroactive polypyrrole (PPy) layer on the anode side is oxidized while that on the cathode side is reduced. Ions can transfer inside the conjugated polymer actuators based on two main mechanisms of diffusion and drift (Madden 2000). Trilayer polypyrrole actuators, which can operate both in air and liquid environments, are promising materials for applications in micromanipulation systems (Wu *et al*. 2006, John et al. 2008).

There are several models in the literature for predicting the behavior and the performance of PPy actuators. According to the literature, the existing models of PPy actuators can be classified into two groups: static and dynamic. Most of the available models in the literature of conductive polymer actuators focus on static operating conditions (Della *et al*. 1997, Christophersen *et al.* 2006, Du *et al.* 2010). Although the static models provide insight into the steady-state analysis of conductive polymer actuators, the design of advanced control systems (Torabi and Amiri Moghadam 2012, Amiri Moghadam *et al.* 2010) and functional devices based on PPy actuators requires dynamic modeling approaches. Thus, the current work extensively focuses on the development of dynamic models for PPy actuators. To study the existing dynamic models, four key factors have been considered: (i) use of physic-based modeling method, (ii) consideration of electrical dynamics, (iii) mechanical dynamics, and (iv) large deformation. These factors play a significant role in the development of dynamic models of PPy actuators, and a model which incorporates all of these factors can predict the performance of PPy actuators more realistically. As the first factor, the physic-based models can be defined as models which are based on physical principles, and in this sense they are superior to black box models which are merely based on data mapping. The next two parameters including (i) the electrical, and (ii) the mechanical dynamic models establish a proper mathematical relation between the input voltage and the output displacement of polymer actuators.

The electrical dynamic or admittance model relates the current, and, therefore, the transferred charge to the input voltage. It is known that the induced actuation force in PPy actuators is directly related to the transferred charge to the actuator. Thus, an electrical admittance model is a necessary component for comprehensive dynamic modeling of PPy actuators. Moreover, mechanical dynamics relate the transferred charge to the bending deformation of PPy actuators, and take into account the mechanical vibration of the actuator. It is evident that a dynamic model which incorporates mechanical dynamics of the actuator can predict the natural frequency of the actuator, and, therefore, can predict the actuator performance in a wider frequency range.

Generally, models which do not take into account both electrical and mechanical dynamics cannot perfectly predict the performance of the PPy actuators and therefore, have a limited application. In our recent work (Amiri Moghadam *et al*. 2012), it was shown that the inclusion of both electrical and mechanical dynamic models is necessary for successful modeling and robust position control of robotic systems based on PPy actuators. The last parameter, the large bending deformation, is the missing part in most of the existing dynamic models. Table 1 compares the available dynamic models in predicting the performance of PPy actuators. It can be seen that there are limited contributions for the comprehensive analysis of conductive polymer actuators, in the sense that most of the existing models use an equivalent electrical circuit to emulate the electrical admittance of the actuator, ignoring the mechanical dynamics (Madden 2000, Madden 2003, Bowers 2004, Fang *et al.* 2008a, b, Shoa *et al*. 2010, Shoa *et al*. 2011, Nguyena 2012). It should be noted that the assumption of constant curvature in these models, only holds for the case of relatively small bending deformation and cannot be applied to the case of large bending deformation. Although the model by (John *et al*. 2010) can predict the mechanical dynamics of the actuator, it is a black box model which cannot establish a relation between the model and the physical parameters of the actuator and, therefore, has a limited application.

Recently, we have proposed two different approaches for dynamic modeling of trilayer polypyrrole bending actuators, which consider both electrical and mechanical dynamics (Amiri Moghadam *et al*. 2011b, 2012, Amiri Moghadam 2012). In the first method, Madden's diffusive elastic metal model (DEM) (Madden 2000) has been further developed by adding a proper mechanical dynamic model based on the finite element technique (Amiri Moghadam *et al*. 2011b). On the other hand, in the second approach, named as analytical-multi-domain-dynamic (AMDD), a complete analytical dynamic model has been proposed (Amiri Moghadam *et al*. 2011c), in which the electrical admittance model of the actuator is obtained based on a distributed RC line, and an effective mechanical dynamic model is derived based on the Hamilton's principle. A common property among the described modeling strategies is that they cannot take into account the geometric nonlinearity of the actuator, whereas, the use of these actuators in functional devices requires nonlinear large deformation dynamic analysis of the system. Addressing the large deformation of polymer actuators, (Mutlu *et al.* 2013a) proposed a kinematic model based on backbone carve theory which considers the PPy actuator as a significant number of rigid links connected by revolute joints. This model, however, cannot take into account either electrical or mechanical dynamics of PPy actuators. Subsequently, in another work (Mutlu *et al*. 2013b), they extended this model by incorporating mechanical dynamics into it. However, this model cannot take into account an electrical admittance of the actuator and instead requires an experimental measuring of the blocking force of the polymer actuators. Moreover, the main assumption for derivation of the induced actuation force in the model is that there is no voltage drop along the length of actuator (Amiri Moghadam *et al.* 2010). This assumption is only true when the actuator is relatively small and, therefore, limits the application of the model. Addressing some deficiencies mentioned and using the rigid finite element (RFE) method, the current work proposes a dynamic model for the large deformation (small strains and moderate rotations) dynamic analysis of polymer actuators. This has been performed by establishing a mathematical relation between the input voltage and the output bending displacement of the polymer actuator, considering both electrical admittance and mechanical dynamics of the actuators simultaneously. In contrast to the classical finite element method (FEM), the RFE method discretizes the flexible links into rigid elements, which facilitates the representation of the inertial features of the body. These elements are connected by means of spring-damping elements (SDEs) (Wittbrodt *et al*. 2006).

Table 1 The comparison of existing dynamic models in predicting the performance of PPy actuators

Authors	Physics-based	Electrical Dynamics	Mechanical Dynamics	Large Deformation
Current work	✓	✓	✓	✓
Mutlu *et al.* 2013b	✓	×	✓	✓
Nguyen *et al.* 2012	✓	✓	×	×
Amiri Moghadam *et al*. 2011c	✓	✓	✓	×
Amiri Moghadam *et al.* 2011b	✓	✓	✓	×
Shoa *et al.* 2011	✓	✓	×	×
Shoa *et al.* 2010	✓	✓	×	×
Fang *et al*. 2008b	✓	✓	×	×
Fang *et al*. 2008a	✓	✓	×	×
Bowers 2003	✓	✓	×	×
Madden 2003	✓	✓	×	×
Madden 2000	✓	✓	×	×

There are several other advantages in applying the RFE method (Wittbrodt *et al*. 2006) such as (i) simplicity, reflected in the description of flexible links as a system of rigid links connected by sdes, (ii) employment of a uniform approach to model rigid and flexible links, (iii) numerical efficiency, and (iv) applicability for the analysis of both small and large deformations. Based on these advantages, we extend the RFE method to emulate the dynamic of polymer actuators, with the actuator being replaced with a set of rigid elements which are connected by means of sdes and controlled by a separate electrical model. In effect, the electrical characteristic of each element is derived based on the ladder network of discrete resistive-capacitive components, with the induced electrochemical moment which acts at each sdes being considered as a linear function of transferred charges to the element. Through numerical simulations, it has been shown that the proposed model works consistently for the experimental data and significantly predicts the behavior of the actuator.

The remainder of the paper has been organized as follows. In Section 2, trilayer PPy actuators are introduced and the synthesis of the polymer actuator has been described. Section 3 presents a dynamic analysis of polymer actuators based on the RFE method proposed. Section 4 validates the model through comparing the experimental results with those generated by the simulation. Concluding g remarks are given in Section 5.

2. Trilayer polypyrrole (PPy) actuators

Trilayer conjugated polymer actuators were electrochemically synthesized and studied for this research. The constitution and geometry of these actuators is depicted in Fig. 1. The actuator consists of a middle porous Polyvinylidene Fluoride (PVDF) layer, which is used as a storage tank for the electrolyte, sandwiched between two PPy layers (Kaynak *et al.* 2011).

The main process responsible for volumetric change of the conjugated polymer actuator is a RedOx reaction. Upon oxidization the PPy layer on the anode side expands, whereas under the same condition, the PPy layer on the cathode side contracts and is reduced as a result. It is this

difference in volume which leads to the bending of the actuator.

2.1 Synthesis of the polymer actuator

Electrochemical polymerization is performed galvanostatically by anodic oxidation of a solution containing the pyrrole monomer and Tetrabutylammonium hexaflurophosphate ($TBAPF_6$) as the dopant in an organic solvent of propylene carbonate (PC). The electrochemical method offers a better control of electrical and mechanical properties (Unsworth *et al.* 1992). Porous polyvinylidene fluoride (PVDF) membranes obtained from Sigma (type) were first vacuum coated with gold using a Balzers sputter coater for 300 seconds. These are used as the working electrode.

A fine stainless steel wire mesh (fine 250) is used as the counter electrode. The deposition of the conducting PPy layer is performed using an electrochemical polymerization cell (Fig. 2) at a constant current density of 0.05 $mAcm^{-2}$ for a period of 12 hours at -10°C. The lower synthesis temperature is found to result in smoother surface morphology and lower surface resistivity (Kaynak 1997). Low temperature electrochemical polymerization results in slower monomer migration in solution. This may slow the oxidation rate of the monomer and polymerization of the anode, thus resulting in smoother surface morphology with lower average surface roughness values (Kaynak 1997).

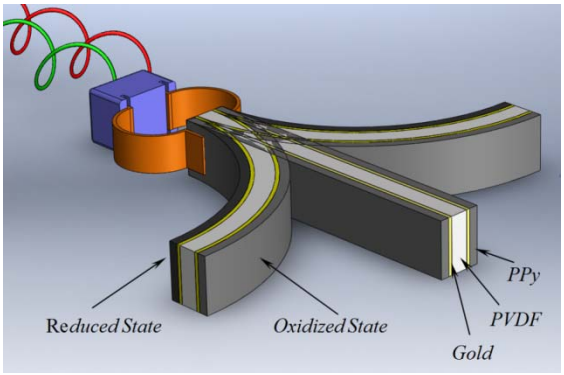

Fig. 1 The diagram of a three-layer polypyrrole actuator

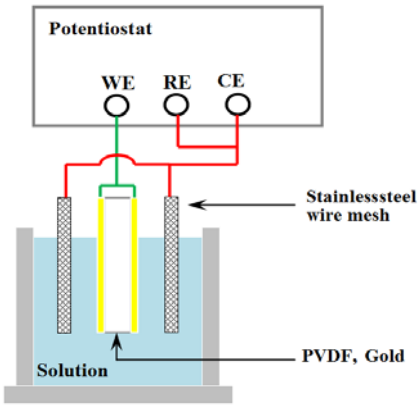

Fig. 2 Electrochemical polymerization cell for fabrication of conductive polymer actuators

The constant current is maintained by using EG&G Princeton Applied Research Model 363 potentiostat/galvanostat. The actuator is rinsed with the polycarbonate solution containing 0.05M $TBA^+ PF_6^-$, and stored in the same solution. Fig. 2 presents the electrochemical polymerization cell which was used to synthesize the polymer actuator.

Fig. 3 shows an SEM image of the cross section of the PC/PF6 actuator. The PPy layer is about 10 μm thick and the PVDF membrane thickness is approximately 80 μm. The gold layer between the PVDF and PPy layers being less than 100 nm thick, was not only too thin but also lacked distinct morphological features to distinguish it in this image. Fig. 4 shows the typical nodular surface morphology of the polypyrrole films that appears on the top and bottom surfaces of the 3 layer actuator. As can be seen in Fig. 4, the surface morphology of this electrochemically synthesized actuator possesses the typical dendritic morphology of PPy films deposited for prolonged times and/or high reactant concentrations (Kaynak 1997). Atomic force microscopy studies have shown that average surface roughness of electrochemically synthesized PPy films increases with dopant concentration, current density, temperature and the duration of deposition (Kaynak 1997).

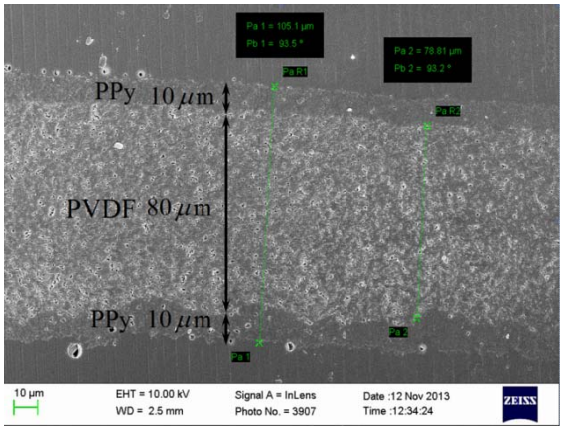

Fig. 3 The SEM image of the cross section of PC/PF6 actuator (showing PVDF and PPy layers)

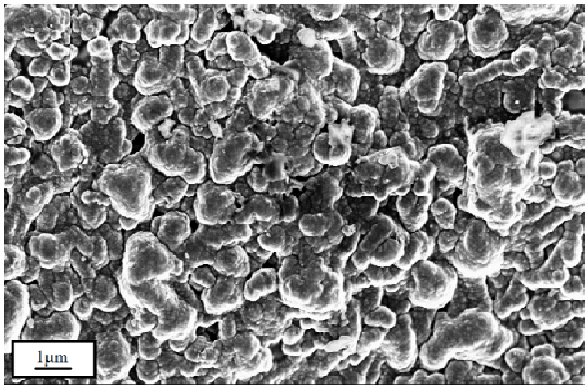

Fig. 4 The SEM image of surface morphology of the polymer actuator, Magnification 25,000X

3. The electromechanical modeling

The electromechanical model used in this paper is comprised of both electrical and mechanical models, and each of these two components is discussed in a separate sub-section

3.1 The electrical modeling

An electrical circuit has been used to model the electrochemical process within the conductive polymer actuator. The electrical charge can be stored within the actuator which is analogous to a capacitance element in an electrical circuit. Additionally, the energy loss in the actuator can be modeled as an electrical resistance. This explains the reason why, in the literature, the simplest lumped electrical model which can describe the electrochemical process within the conductive polymer actuators is an RC circuit (Madden 2000). It has been shown that the major mechanism which is responsible for ion transport within the conductive polymer actuator is diffusion (Daum *et al.* 1980). Considering the above assumption, (Madden 2003) proposed a continuum electrical admittance model for polymer actuators which is known as the diffusive elastic metal model (DEM). (Fang et al. 2008a) obtained the electrical admittance model of trilayer polymer actuators utilizing DEM.

Several authors have proposed that the transport of ions within the polymer can be modeled by a finite transmission line (Amemiya *et al*. 1993, Warren 2005, Tso *et al*. 2007, Punning 2007, Kaal *et al*. 2010, Haus *et al*. 2013). In our previous work, we have demonstrated that a finite RC transmission line can model the electrical admittance of the trilayer polymer actuators (Amiri Moghadam *et al.* 2011c) and it resembles Madden's diffusive elastic metal model (Madden 2000). However, the main issue regarding our previous work is that it can only emulate the ion movement through the thickness of PPy actuators. In other words, this model assumes that there is no voltage drop along the length of the polymer actuator. However, this assumption holds only for relatively small actuators. The direct consequence of this assumption is that the actuators model always bends as a perfectly circular curve (constant-curvature). However, experimental observation in the current work shows that the curvature of the actuator decreases along its length, away from the power source, suggesting that there is a drop of potential along the length of the actuator due to the surface resistance of the PPy layers. With this in mind, in the current work we utilize a discrete electrical circuit model to emulate the electrical admittance of the actuator with consideration of voltage drop along the actuator length. Fig. 5 shows the proposed electrical model which is a ladder network of discrete resistive-capacitive components. It is evident that, when the number of used elements in the model moves towards infinity, the proposed model will be transformed to a transmission line model. The discrete representation of the actuator facilitates the RFE modeling with respect to fully consider both electrical and mechanical characteristics of the corresponding elements.

According to Fig. 5, resistances r_a and r_b in each element represent the surface resistance of top and bottom polypyrrole layers, respectively. Although the resistance values for the top and bottom PPy layers should not have any significant difference, different resistance variables are incorporated into the model to cater for coatings of different thickness and conductivity values. In our experiments, the positioning of the sample in the electrochemical cell and careful monitoring of the electrochemical parameters enabled a uniform coating on both sides of the PVDF film and hence there were no significant difference in the resistance values. These two parameters clearly account for voltage drop along the length of the actuators. Moreover, resistance R_2 and capacitance

c emulate the dynamic of ions movement through the thickness of the actuators. For the sake of simplicity, the discrete electrical network in Fig. 5 can be transferred into its equivalent model in Fig. 6 by replacing $R_1 = r_a + r_b$. According to Fig. 6 and Kirchhoff's and Ohm's laws, one can analyze the electrical model of the actuator based on following sets of recursive equations

$$\begin{cases} I_H^{(i+1)} = I_H^{(i)} - I_V^{(i)} \\ V^{(i+1)} = V^{(i)} - I_H^{(i+1)} R_1 \\ I_V^{(i+1)} = V^{(i+1)} / (R_2 + 1/cs) \end{cases} \quad (1)$$

where, *s* is Laplace variable, $V^{(i)}$ is the voltage of ith element, $I_H^{(i)}$ is the current that passes through the resistor R_1 in ith element, and $I_V^{(i)}$ is the current that follows through *c*-R_2 branch in ith element.

It is important to include an electrical resistance along the length of the sample to generalize our model so that any potential drop along the sample is taken into account. For example for the cases where there is no gold layer in the actuator or the actuator is relatively long, there would be a significant potential drop along the actuator length (Shoa *et al*. 2010, 2011). The gold coating is performed on the porous surface of PVD, and as a result there may be discontinuities in gold coating which may result in lower resistivity than anticipated. The gold layer is deposited on the PVDF film and situated underneath the PPy layer, while the electrical contacts are attached to the outer PPy surface

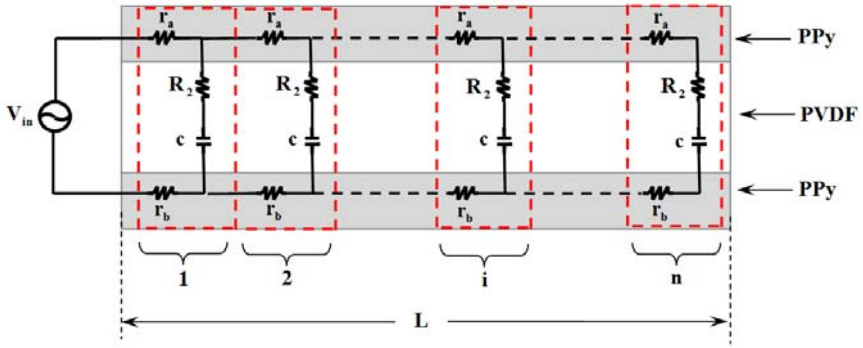

Fig. 5 The equivalent discrete electrical circuit for the polymer actuator

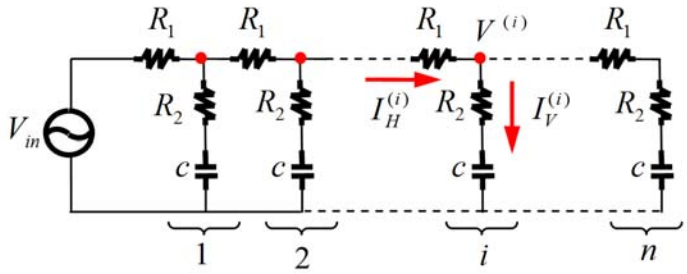

Fig. 6 Simplified discrete electrical network model of the polymer actuator

Considering that five elements are used for simulation of the electrical model, the electrical admittance of the actuator is

$$\frac{I_t}{V_{in}} = \frac{\eta_5 s^5 + \eta_4 s^4 + \eta_3 s^3 + \eta_2 s^2 + \eta_1 s}{\mu_5 s^5 + \mu_4 s^4 + \mu_3 s^3 + \mu_2 s^2 + \mu_1 s \ +1} \tag{2}$$

where, I_t is the total current in the equivalent electrical circuits, and model parameters are presented in the Appendix. Furthermore, the charging current in each element can be obtained as

$$\frac{I_V^{(1)}}{V_{in}} = \frac{\lambda_{51} s^5 + \lambda_{41} s^4 + \lambda_{31} s^3 + \lambda_{21} s^2 + \lambda_{11} s}{\mu_5 s^5 + \mu_4 s^4 + \mu_3 s^3 + \mu_2 s^2 + \mu_1 s \ +1} \tag{3a}$$

$$\frac{I_V^{(2)}}{V_{in}} = \frac{\lambda_{52} s^5 + \lambda_{42} s^4 + \lambda_{32} s^3 + \lambda_{22} s^2 + \lambda_{12} s}{\mu_5 s^5 + \mu_4 s^4 + \mu_3 s^3 + \mu_2 s^2 + \mu_1 s \ +1} \tag{3b}$$

$$\frac{I_V^{(3)}}{V_{in}} = \frac{\lambda_{53} s^5 + \lambda_{43} s^4 + \lambda_{33} s^3 + \lambda_{23} s^2 + \lambda_{13} s}{\mu_5 s^5 + \mu_4 s^4 + \mu_3 s^3 + \mu_2 s^2 + \mu_1 s \ +1} \tag{3c}$$

$$\frac{I_V^{(4)}}{V_{in}} = \frac{\lambda_{54} s^5 + \lambda_{44} s^4 + \lambda_{34} s^3 + \lambda_{24} s^2 + \lambda_{14} s}{\mu_5 s^5 + \mu_4 s^4 + \mu_3 s^3 + \mu_2 s^2 + \mu_1 s \ +1} \tag{3d}$$

$$\frac{I_V^{(5)}}{V_{in}} = \frac{\lambda_{55} s^5 + \lambda_{45} s^4 + \lambda_{35} s^3 + \lambda_{25} s^2 + \lambda_{15} s}{\mu_5 s^5 + \mu_4 s^4 + \mu_3 s^3 + \mu_2 s^2 + \mu_1 s \ +1} \tag{3e}$$

where the model parameters are presented in the appendix. It must be noted that resistance R_1 can be measured experimentally according to the surface resistance of polypyrrole layers. Through experimental measurements, the resistivity of the polypyrrole layers is obtained to be 8.8333×10^{-5} Ωm which is in the typical range (Fang *et al*. 2008a). Based on this value, it is straightforward to obtain the value of R_1 as follows

$$R_1 = (\rho_{top} + \rho_{bottom}) \frac{L}{n \ b \ h_{PPy}} = 15.9 \ \Omega \tag{4}$$

where ρ_{top} and ρ_{bottom} are resistivity of the top and the bottom polypyrrole layers, respectively, and n is number of used terms in the electrical model. Moreover, L, b, and h_{PPy} are length, width, and thickness of polypyrrole layer respectively. Parameters R_2 and c are identified by means of simulated annealing method which is one of the most efficient random search algorithms for obtaining the global minimum (Collins *et al*. 1988). The error signal is defined as the difference between the experimental and simulated current output of the actuator, and consequently the objective function is defined as the integral of squared relative error. Moreover, the vector of unknown parameters $\boldsymbol{\gamma}$ is defined as

$$\boldsymbol{\gamma} = [R_2, c]^T \tag{5}$$

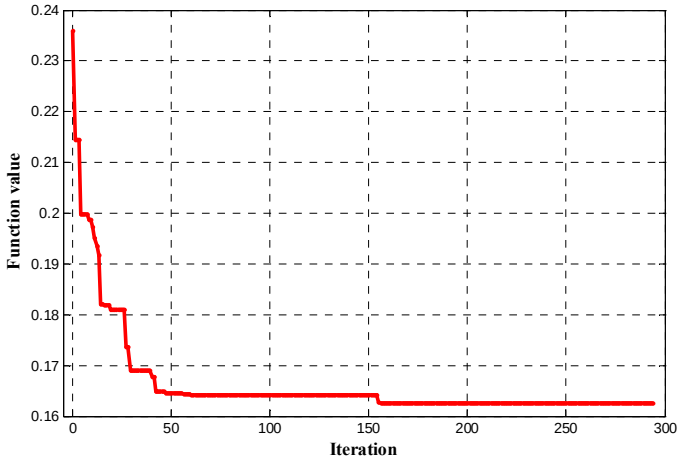

Fig. 7 Convergence of the objective function based on the simulated annealing algorithm

According to Fig. 7, it can be observed that the objective function converges after approximately 150 iterations, and unknown parameters are identified to be R_2= 1530 Ω and c=0.0013 F.

3.2 The mechanical modeling

In contrary to the electrical model which relates the current to the stored charges, the mechanical model relates the stored charges to the bending displacement of the PPy actuators. As stated earlier, three-layer polymer actuators can bend based on the expansion and contraction of the top and bottom layers, with the induced levels of stress in the expanded and contracted layers being assumed to be the same but in the opposite directions. The basic idea in the mechanical modeling part is to consider the polymer actuator as a discretized system which consists of rigid finite elements (rfes) connected by spring–damping elements (sdes), in which each rigid finite element moves based on the induced electrochemical moment, denoted by $M_{ch}^{(i)}$ acting at $rfe^{(i)}$. As shown in Fig. 8, the actuator is divided into (n+1) rfes and (n) sdes. The components $rfe^{(i)}$ and $rfe^{(i-1)}$ are considered to be connected by means of revolute joint at $sde^{(i)}$. Moreover, sdes comprise of rotational stiffness ($k^{(i)}$) and damping elements ($c^{(i)}$). These parameters will be introduced later in this section. It has been experimentally shown that the induced electrochemical strain in polymer actuators is linearly related to the density of the transferred charges (Madden 2000). Moreover, the induced electrochemical moment is a linear function of transferred charges to the actuator (Amiri Moghadam 2011b). That is why we have defined the induced electrochemical moment in the ith element as follows.

$$M_{ch}^{(i)}(t) = \alpha \int_0^t I_V^{(i)}(t)\, dt \tag{6}$$

where α is the moment-to-charge ratio.

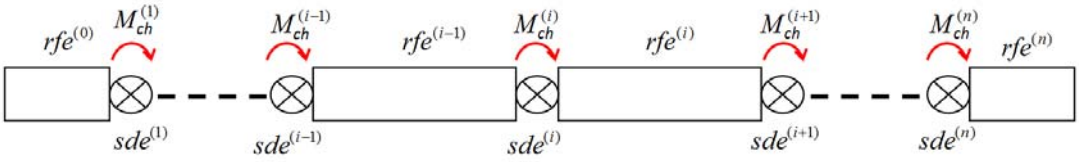

Fig. 8 The discretization of a three-layer PPy actuator into rfes and sdes

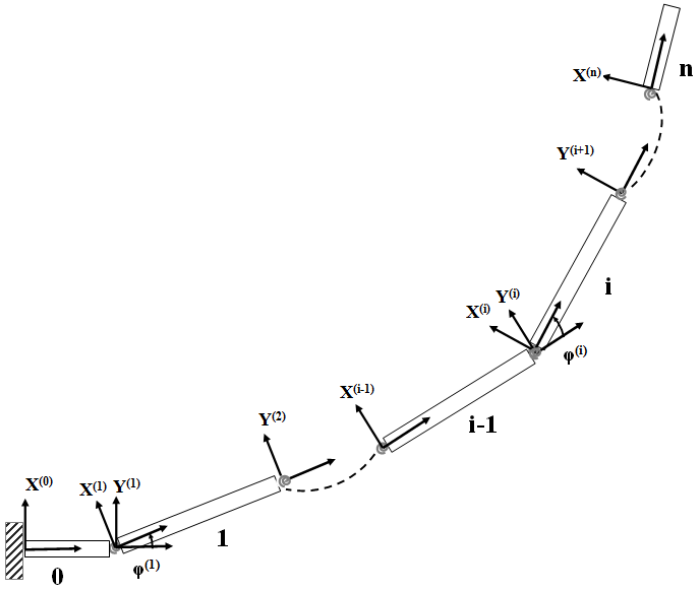

Fig. 9 The frame assignment for *rfes* and *sdes*

Now the motion of components (rfes) can be studied by assigning suitable generalized coordinates to them. According to Fig. 9, the coordinate system $\{X^{(i)}\}$ and $\{Y^{(i)}\}$ are attached to $rfe^{(i)}$ and $sde^{(i)}$. It must be noted that the orientation of the coordinate system $\{Y^{(i)}\}$ coincides with the coordinate system $\{X^{(i-1)}\}$. Thus, the transformation matrix which defines the frame $\{X^{(i)}\}$ relative to the frame $\{X^{(i-1)}\}$ is expressed as

$$\widetilde{\mathbf{B}}^{(i)} = \begin{bmatrix} \cos(\varphi^{(i)}) & -\sin(\varphi^{(i)}) & d^{(i)} \\ \sin(\varphi^{(i)}) & \cos(\varphi^{(i)}) & 0 \\ 0 & 0 & 1 \end{bmatrix} \tag{7}$$

where, $\varphi^{(i)}$ is the angle between these two frames. Considering that the actuator has a length of L and it has been divided into ($n+1$) rfes, the value of $d^{(i)}$ can be calculated through the following relation.

$$d^{(1)} = L/2n, \quad d^{(i)} = L/n \qquad i = 2,3,\ldots,n. \tag{8}$$

With this in mind, the transformation matrix which defines the frame $\{X^{(i)}\}$ relative to the frame $\{X^{(0)}\}$ is

$$\mathbf{B}^{(i)} = \widetilde{\mathbf{B}}^{(1)}\,\widetilde{\mathbf{B}}^{(2)}\ldots\,\widetilde{\mathbf{B}}^{(i)} \qquad i = 1,2,\ldots,n. \tag{9}$$

Consequently, the position of any particle dm in $rfe^{(i)}$ with respect to the frame $\{X^{(0)}\}$ is defined as

$$\mathbf{r}^{(i)} = \mathbf{B}^{(i)}\,\widetilde{\mathbf{r}}^{(i)} \qquad i = 1,2,\ldots,n. \tag{10}$$

where $\widetilde{\mathbf{r}}^{(i)} = [\widetilde{x}_1^{(i)}\ \widetilde{x}_2^{(i)}\ 1]^T$ and $\mathbf{r}^{(i)} = [x_1^{(i)}\ x_2^{(i)}\ 1]^T$ are the position vector of the particle dm relative to frame $\{X^{(i)}\}$ and $\{X^{(0)}\}$, respectively. Therefore, the kinetic energy of the particle dm is represented as

$$dT^{(i)} = \frac{1}{2} tr\left\{\dot{\mathbf{r}}^{(i)}\,\dot{\mathbf{r}}^{(i)^T}\right\} dm^{(i)} \quad i = 1,2,\ldots,n. \tag{11}$$

It follows that the kinetic energy of the $rfe^{(i)}$ is obtained as

$$T^{(i)} = \frac{1}{2}\int_{m^{(i)}} tr\left\{\dot{\mathbf{r}}^{(i)}\,\dot{\mathbf{r}}^{(i)^T}\right\} dm^{(i)} = \frac{1}{2}\int_{m^{(i)}} tr\left\{\dot{\mathbf{B}}^{(i)}\,\widetilde{\mathbf{r}}^{(i)}\,\widetilde{\mathbf{r}}^{(i)^T}\,\dot{\mathbf{B}}^{(i)^T}\right\} dm^{(i)}$$

$$= \frac{1}{2} tr\left\{\dot{\mathbf{B}}^{(i)}\left[\int_{m^{(i)}} \widetilde{\mathbf{r}}^{(i)}\,\widetilde{\mathbf{r}}^{(i)^T} dm^{(i)}\right]\dot{\mathbf{B}}^{(i)^T}\right\} = \frac{1}{2} tr\left\{\dot{\mathbf{B}}^{(i)}\,\mathbf{H}^{(i)}\,\dot{\mathbf{B}}^{(i)^T}\right\} \qquad i = 1,2,\ldots,n. \tag{12}$$

where $H^{(i)}$ is the pseudo-inertia matrix, which is defined as

$$H^{(i)} = \int_{m^{(i)}} \widetilde{\mathbf{r}}^{(i)}\,\widetilde{\mathbf{r}}^{(i)^T} dm^{(i)} \qquad i = 1,2,\ldots,n. \tag{13}$$

Thus, the kinetic energy can be rewritten as

$$T^{(i)} = \frac{1}{2} tr\left\{\dot{\mathbf{B}}^{(i)}\,\mathbf{H}^{(i)}\,\dot{\mathbf{B}}^{(i)^T}\right\} \qquad i = 1,2,\ldots,n. \tag{14}$$

Finally, the kinetic energy of the actuator is determined by summing over all *rfes*

$$T = \sum_{i=1}^{n} T^{(i)} \tag{15}$$

The potential energy of the rotational springs at *sdes* is expressed as

$$V = \sum_{i=1}^{n} \frac{1}{2} k^{(i)} \left[\varphi^{(i)}\right]^2 \tag{16}$$

where $k^{(i)}$ is the coefficient of rotational stiffness.

$$D = \sum_{i=1}^{n} \frac{1}{2} c^{(i)} \left[\dot{\varphi}^{(i)}\right]^2 \tag{17}$$

where $c^{(i)}$ is the coefficient of rotational damping. The parameter of *sdes* (i.e., rotational stiffness and damping coefficients) can be obtained from analyzing a beam section with the length of ΔL (Wittbrodt *et al.* 2006). The value of stress along the segment ΔL can be calculated through the following relation.

$$\sigma(t) = E\,\varepsilon(t) + \eta\,\dot{\varepsilon}(t) \tag{18}$$

In this relation, $\varepsilon(t)$ is the strain rate, E is the Young's modulus, and η is the normal damping material constant. Fig. 10 shows the bending deformation of the beam segment and its equivalent *sde*. According to this figure, the value of the strain can be calculated as

$$\varepsilon(t) = \frac{y\,\Delta\theta}{\Delta L} \tag{19}$$

Thus, the bending moment can be obtained as

$$M(t) = \int_A \frac{E\,y^2\,\Delta\theta}{\Delta L} dA + \int_A \frac{\eta\,y^2\,\Delta\dot{\theta}}{\Delta L} dA \tag{20}$$

where, A is the area of beam cross-section. By integrating the above equation we obtain

$$M(t) = \frac{E\,I}{\Delta L}\Delta\theta + \frac{\eta\,I}{\Delta L}\Delta\dot{\theta} \tag{21}$$

where, I is the area moment of inertia of the beam. Moreover the bending moment in equivalent *sde* is

$$M(t) = k^{(i)}\Delta\theta + c^{(i)}\Delta\dot{\theta} \tag{22}$$

It must be noted that when ΔL is equal to the element length (L/n), the bending angle $\Delta\theta$ becomes equal to $\varphi^{(i)}$ and therefore, by comparing Eqs. (21) and (22), parameters of *sde* are defined as (Wittbrodt *et al*. 2006)

$$k^{(i)} = \frac{n\,E\,I}{L} \tag{23a}$$

$$c^{(i)} = \frac{n\,\eta\,I}{L} \tag{23b}$$

The virtual work which is done by induced electro chemical moment is defined as

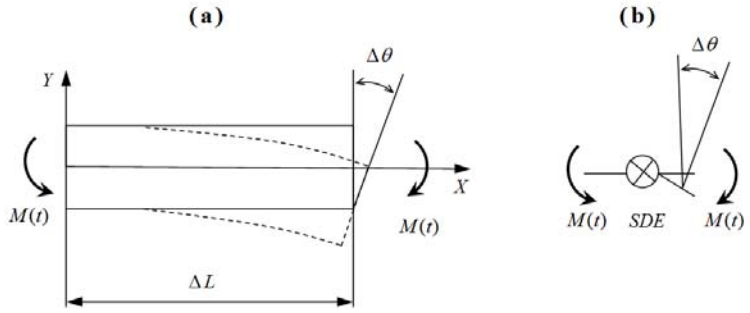

Fig. 10 Bending deformation: (a) beam segment, (b) equivalent spring-damping element

$$\delta W = \delta \left[\sum_{i=1}^{n} M(t)_{ch}^{(i)} \varphi^{(i)} \right] \tag{24}$$

Thus, the generalized forces ($Q^{(i)}$) is obtained as

$$Q^{(i)} = M(t)_{ch}^{(i)} \qquad i = 1, 2, \ldots, n. \tag{25}$$

Next, based on Lagrange's equations, the discrete set of equations that describe the dynamic of the actuator is derived as follows

$$\frac{d}{dt}\left(\frac{\partial T}{\partial \dot{q}_i}\right) - \frac{\partial T}{\partial q_i} + \frac{\partial V}{\partial q_i} + \frac{\partial D}{\partial \dot{q}_i} = Q^{(i)} \qquad i = 1, 2, \ldots, n. \tag{26}$$

where the vector of generalized coordinates, $\mathbf{q}$, is defined as

$$\mathbf{q} = [\varphi^{(1)}, \varphi^{(2)} \ldots, \varphi^{(n)}]^T \tag{27}$$

Finally, the equations of motion can be rewritten in the compact matrix form as

$$\mathbf{A}(t)\,\ddot{\mathbf{q}} + \mathbf{e}(q, \dot{q}, t) + \mathbf{C}\,\dot{\mathbf{q}} + \mathbf{K}\,\mathbf{q} = \mathbf{Q}(t) \tag{28}$$

Where

$$\mathbf{A}(t) = [a_{ij}], \quad a_{ij} = \sum_{k=\max\{i,j\}}^{n} tr\left\{ \frac{\partial \mathbf{B}^{(k)}}{\partial q_i} \mathbf{H}^{(k)} \left(\frac{\partial \mathbf{B}^{(k)}}{\partial q_j} \right)^T \right\} \tag{29}$$

$$\mathbf{e}(q, \dot{q}, t) = \{e_i\}, \quad e_i = \sum_{k=i}^{n} tr\left\{ \frac{\partial \mathbf{B}^{(k)}}{\partial q_i} \mathbf{H}^{(k)} \left(\sum_{h=1}^{k} \sum_{j=1}^{k} \frac{\partial^2 \mathbf{B}^{(k)}}{\partial q_h \partial q_j} \dot{q}_h \dot{q}_j \right)^T \right\} \tag{30}$$

$$\mathbf{C} = diag\left\{ c^{(1)}, c^{(2)}, \ldots, c^{(n)} \right\} \tag{31}$$

$$\mathbf{K} = diag\left\{k^{(1)}, k^{(2)}, \ldots, k^{(n)}\right\} \tag{32}$$

4. Comparison of experimental and simulation results

For validating the model, we compared the experimental results with those generated as a result of predicting the behavior of the actuator by the model. For this purpose, as shown in Fig. 11, a 0.1 mm × 2 mm × 18 mm PC/PF6 actuator was employed, and a known voltage was supplied to the actuator by means of a potentiostat. To make the validation more accurate and robust, both square and sine input voltage waves were employed. The waves were generated, through a function generator, and supplied to the actuator. A Keithley 2400 source meter was used to measure the current output of the actuator, and the actuator motion was recorded by a Canon full frame digital camera fitted with a macro lens. Numerical simulations were performed using MATLAB software. Since the proposed model is comprised of electrical and mechanical parts, both current and displacement outputs of the actuator were measured so that both electrical and mechanical models can be validated.

For both square and sine input voltage waves, five elements were considered for the simulation of the electrical model. Considering the charging current in each element, ($I_V^{(i)}$), the total output current of the actuator ($I_t = \sum_{i=1}^{n} I_V^{(i)}$) was calculated. First, the response of the actuator to the square wave input voltage was measured. Fig. 12 shows the charging current in each element. It is worth mentioning that the curvature of the actuator decreases (Fig. 11) along its length, away from the power source, suggesting that there is a drop of potential along the length of the actuator due to the surface resistance of the PPy. Based on this observation, we used a discrete set of resistors and capacitors to model the electrical admittance of the actuator. Fig. 12 shows that the element closest to the power source has the highest current. Conversely, the element furthest away from the power source has the lowest current. The charging current in turn, exhibits an exponential decrease with time as our model is based on ladder network of discrete resistive-capacitive components. Fig. 13 compares the overall current of the theoretical model with the experimental current. It can be seen that the model shows a good match with the experimental results. Moreover, a sine wave input voltage can be used to further analyze the electrical model.

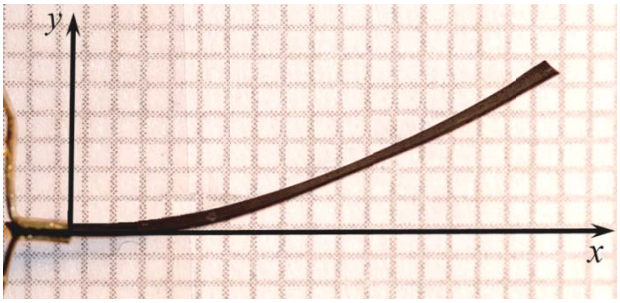

Fig. 11 Frame assignment and bending deformation of PC/PF6 actuator

Fig. 14 shows the charging current in each element and Fig. 15 compares the overall current of the theoretical model against the experimentally measured current. It can be seen that the shape of theoretical current is almost the same as the shape of the experimental current and is in agreement with experimental data. However, the experimental current shows a slight distortion from the ideal sine-wave shape indicating that the current voltage relation can be nonlinear. In our future work, this can be investigated thoroughly, examining the application of sophisticated nonlinear circuits for analyzing the actuator electrical model.

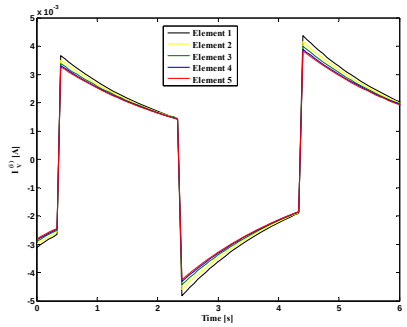

Fig. 12 The simulated current through each C-R_2 branch ($I_V^{(i)}$)

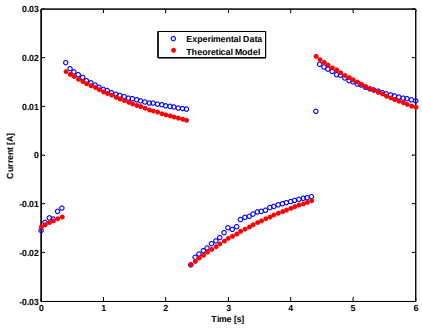

Fig. 13 The comparison of overall simulated current of polymer actuator and experimental current under the square wave input voltage

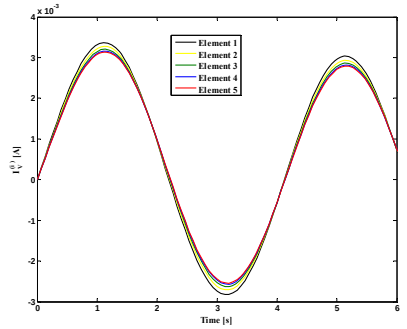

Fig. 14 The simulated current through each C-R_2 branch ($I_V^{(i)}$)

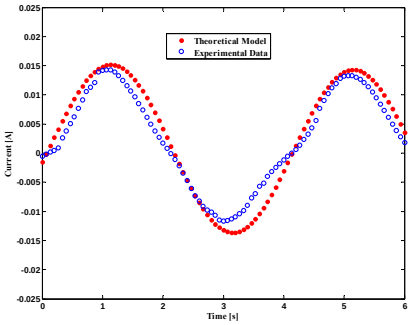

Fig. 15 The comparison of overall simulated current of polymer actuator and experimental current under the sine wave input voltage

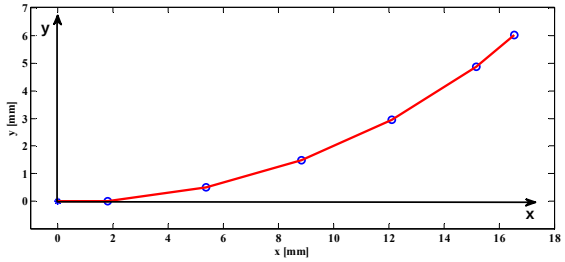

Fig. 16 Five degrees of freedom RFE mechanical model of the actuator

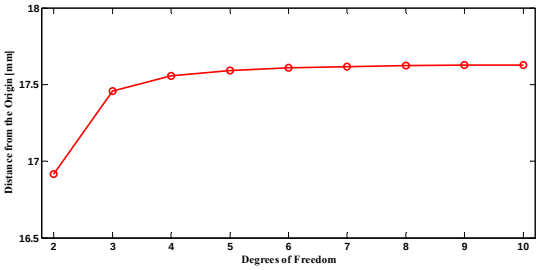

Fig. 17 The actuator tip distance from the origin of the Cartesian coordinate system

Now, let us examine the bending displacement of the actuator. According to Fig. 16, a mechanical model with 5 degrees of freedom (DOF) was utilized for simulation purpose. Large bending deformations of up to 6 mm were observed in experimental data. Thus, we studied the convergence of the mechanical model for predicting a 6 mm bending displacement. For this purpose, the actuator tip distance from the origin of the Cartesian coordinate system for using different numbers of elements was calculated. It can be seen from Fig. 17 that the mechanical model converges as the number of elements increases. However, the increase in the number of elements amplifies the computational load. Thus, a model with 5 DOF which shows an approximate convergence was utilized for numerical simulations.

In validating the mechanical model, again both square and sine input voltage waves were considered. In this validation, the bending angle in each element ($\varphi^{(i)}$) and the bending displacement of the actuator tip were calculated. First, the results for the square wave input voltage is presented. Fig. 18 shows the bending angle in each element and Fig. 19 shows the comparison of the overall simulated actuator tip displacement and experimental bending displacements. It can be observed that the simulation results are in a good agreement with experimental data. Similar to the electrical model, it can be seen that the bending angle decreases along the length of the actuator. Element 1 being closest to the power source has the largest bending angle whereas Element 5 being furthest away from the power source has the smallest bending angle.

The mechanical model can be further analyzed in response to a sine wave input voltage. Fig. 20 shows the bending angle in each element and Fig. 21 shows a comparison of the overall simulated actuator tip displacement and experimental bending displacements. It can be observed that the simulation results are in good agreement with experimental data.

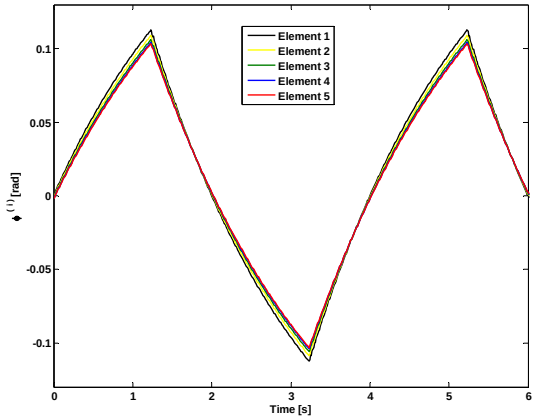

Fig. 18 The bending angle associated with each element ($\varphi^{(i)}$)

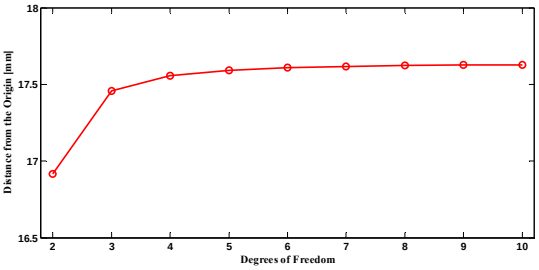

Fig. 19 The comparison of the results produced by the overall theoretical model against the experimental bending displacement of the actuator tip in response to the square wave input voltage

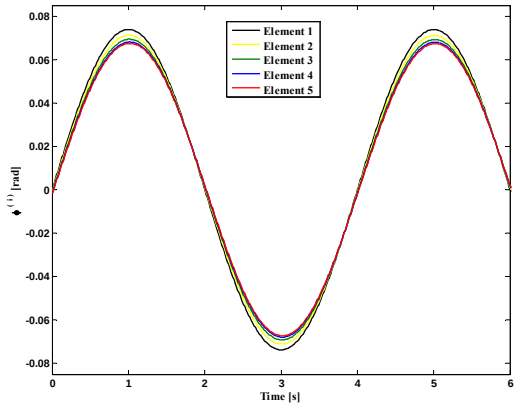

Fig. 20 The bending angle associated with each element ($\varphi^{(i)}$)

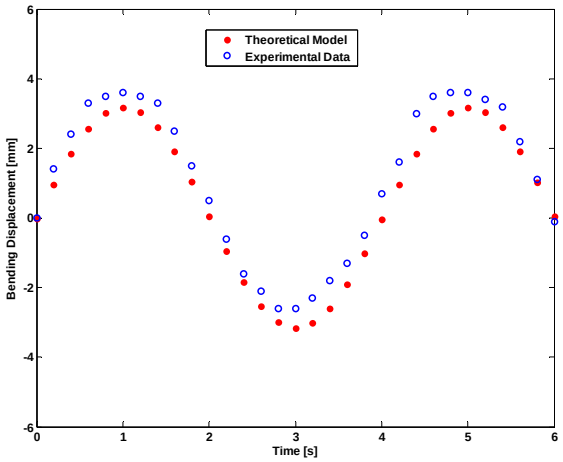

Fig. 21 The comparison of the results produced by the overall theoretical model against the experimental bending displacement of the actuator tip in response to the sine wave input voltage

Since the proposed modeling approach takes into account mechanical dynamics of the actuator, it would be interesting to study the frequency domain response of the actuator. Fundamental natural frequency of the actuator was observed to be around 39.5 Hz. Figs. 22 and 23 show the bending angle in each element and bending displacement of the actuator model in response to a sine wave input voltage with the frequency of 39.5 Hz. According to these figures, it is evident that the amplitude of the vibration increases at the fundamental natural frequency of the actuator which is consistent with the experimental data. As it is anticipated, at fundamental natural frequency, the role of mechanical dynamic model becomes dominant, in which case the inertial effects to the bending angle are taken into account. The large deviation of each subsequent element is due to the dominant role of the mechanical inertial dynamics. This is a reasonable outcome as inertial effects of each element cumulatively contribute to bending angle from tip towards the fixed end of the actuator.

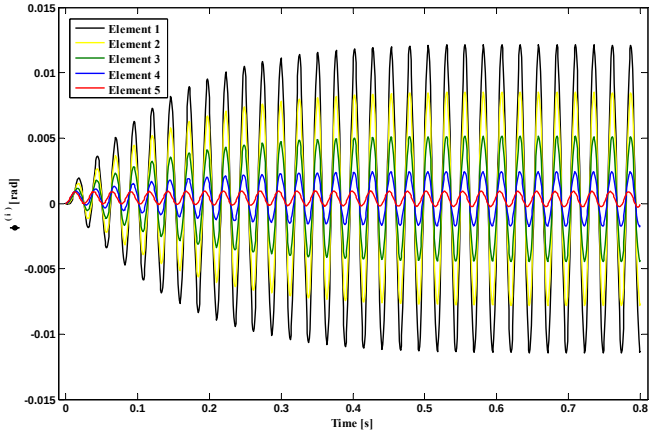

Fig. 22 The simulated bending angle in each element ($\varphi^{(i)}$) of the actuator in response to a sine wave input voltage with the frequency of 39.5 Hz

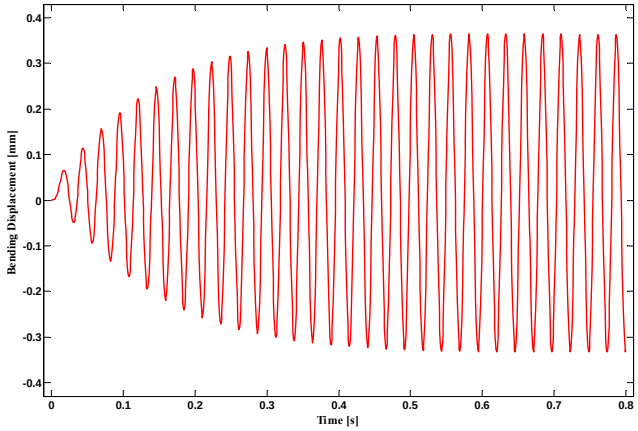

Fig. 23 The simulated total bending displacement of the tip of the actuator in response to a sine wave input voltage with the frequency of 39.5 Hz

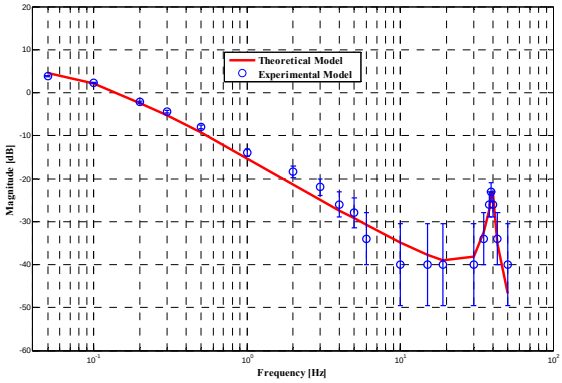

Fig. 24 The comparison of the experimental and theoretical frequency response of the actuator

Moreover, Fig. 24 compares theoretical and experimental magnitude Bode plot of the actuator. It is evident that the theoretical model can predict the frequency response of the actuator well. A point worth noticing is that, as the frequency is increased, the displacement is decreased. This may be attributed to the slowing down of the rate of diffusion of PF_6 and solvent ions at higher frequencies through the PVDF, between polypyrrole layers.

5. Conclusions

With a wide scope of applications of polymer actuators from biomimetic robots through biomedical microdevices to artificial organs, the study of their behavior under different shape of voltages is of paramount importance. In this paper, a nonlinear dynamic model for analysis of large bending deformation (small strains and moderate rotations) of polymer actuators was proposed. The model establishes a mathematical relation between the input voltage and the output bending displacement of the polymer actuator. The effectiveness of the model arises from integrating a ladder network of discrete components with the rigid finite element (RFE) method. The modeling technique based on RFE provides a unified approach to analyze micro robotic systems which consist of both flexible polymer links and rigid links. This important feature, will enhance design and modeling of functional devices based on conductive polymer actuators. The proposed model can be considered as a step forward towards understanding the large deformation dynamic behavior of conducting polymer actuators based on their physical parameters. It must be noted that the proposed modeling strategy can be simply extended to other polymer actuators such as ionic polymer conductor network composite (IPCNC) actuators with some modifications in the electrical dynamic model (Amiri Moghadam *et al.* 2014).

Simulation results for both square and sine wave input voltages indicate that both electrical and mechanical models are in good agreement with the experimental data. Moreover, frequency domain analysis of the actuator indicates that the proposed model can predict natural frequency and frequency response of the actuator well. The type of nonlinearity which was considered in this work was geometric nonlinearity (i.e., large deformation). However, other sources of nonlinearities can be observed in polymer actuators. For instance, in the electrical domain, the relation between the current and voltage is nonlinear and in the mechanical domain, there is a material nonlinearity. In our future work, other sources of nonlinearities can be observed and the current model can be enhanced to handle other cases.

References

Amemiya, T., Hashimoto, K. and Fujishima, A. (1993), "Frequency-resolved faradaic processes in polypyrrole films observed by electromodulation techniques: electrochemical impedance and color impedance spectroscopies", *J. Phys. Chem*., **97**(16), 4187–4191.

Amiri Moghadam, A.A., Moavenian, M. and Torabi, K., (2010), "Takagi-Sugeno fuzzy modelling and parallel distribution compensation control of conducting polymer actuators", *J. Syst. Control Eng*., **224**(1), 41-51.

Amiri Moghadam, A.A., Moavenian, M. and Ekhteraei Tousi, H. (2011a), "Modeling and robust control of a soft robot based on conjugated polymer actuators", *Model. Iden. Control*, **14**(3), 216-226.

Amiri Moghadam, A.A., Torabi, K. and Moavenian, M. (2011b), "Finite element modeling and robust control of fast trilayer polypyrrole bending actuators", *Int. J. Appl. Electrom*., **35,** 281-305.

Amiri Moghadam, A.A., Moavenian, M., Torabi, K. and Tahani, M. (2011c), "Analytical dynamic modeling of fast trilayer polypyrrole bending actuators", *Smart Mater. Struct*., **20**(11), 1-9.

Amiri Moghadam. A.A. (2012), *Dynamic modeling and robust control of a micro robot based on fast trilayer polypyrrole*, Ph.D. Dissertation, Ferdowsi University of Mashhad, Mashhad.

Amiri Moghadam, A.A., Torabi, K., Moavenian, M. and Davoodi, R. (2012), "Dynamic modeling and robust control of an l-shaped micro robot based on fast trilayer polypyrrole bending actuators", *J. Intel. Mat. Syst. Str*., **24**(4), 484-498.

Amiri Moghadam, A.A., Hong, W., Kouzani, A., Kaynak, A., Zamani, R. and Montazami, R. (2014), "Nonlinear dynamic modeling of ionic polymer conductive network composite actuators using rigid finite element method", *Sensor. Actuat. A*, DOI: 10.1016/j.sna.2014.07.012.

Bar-Cohen, Y., Xue, T., Shahinpoor, M., Simpson, J. and Smith, J. (1998), "Flexible, low-mass robotic arm actuated by electroactive polymers and operated equivalently to human arm and hand", *Proceedings of the 3rd Conf. on Robotics for Challenging Environments,* Albuquerque, New Mexico, USA.

Bar-Cohen, Y. (2001), *Electroactive polymer (eap) actuators as artificial muscles: reality, potential, and challenges*, SPIE, Bellingham, WA, USA.

Bowers, T.A. (2004), *Modeling, simulation, and control of a polypyrrole-based conducting polymer actuator*, PhD Dissertation, MIT, Massachusetts.

Carpi, F. and Smela, E. (2009), *Biomedical Applications of Electroactive Polymer Actuators,* London, UK, John Wiley & Sons Ltd.

Chen, Z., Shatara, S. and Tan, X. (2010), "Modeling of biomimetic robotic fish propelled by an ionic polymer–metal composite caudal fin", *IEEE/ASME T. Mechatron*., **15,** 448-59.

Christophersen, M., Shapiro, B. and Smela, E. (2006), "Characterization and modelling of PPy bilayer microactuators. Part 1. Curvature", *Sensor. Actuat. B – Chem.*, **115**, 596-609.

Collins, N.E., Eglese, R.W. and Golden, B.L. (1988), "Simulated annealing-An annotated bibliography", *Am. J. Mathematical Management Sci.*, **8**, 209-308.

Daum, P., Lenhard, J.R., Rolison, D. and Murray, R.W. (1980), "Diffusional charge transport through ultrathin films of radiofrequency plasma polymerized vinylferrocene at low temperature", *J. Am. Chem. Soc*., **102**(14), 4649-4653.

Della Santa, A., De Rossi, D. and Mazzoldi, A. (1997), "A Characterization and modeling of a conducting polymer muscle-like linear actuator", *Smart Mater. Struct*., **6**(1), 23-34.

Du, P., Lin, X. and Zhang, X. (2010), "A multilayer bending model for conducting polymer actuators", *Sensor. Actuat. A- Phys.*, **163**(1), 240-246.

Fang, Y., Tan, X., Shen, Y., Xi, N. and Alici, G. (2008a), "A scalable model for trilayer conjugated polymer actuators and its experimental validation", *Mater. Sci. Eng*., **28**(3), 421-428.

Fang, Y., Tan, X. and Alici, G. (2008b), "Redox level-dependent impedance model for conjugated polymer actuators", *Sensor. Actuat. B – Chem*., **132**(1), 182-190.

Hara, S., Zama, T., Takashima, W. and Kaneto, K. (2005), "Free-standing gel-like polypyrrole actuators doped with bis (perfluoroalkylsulfonyl) imide exhibiting extremely large strain", *Smart Mater. Struct*., **14**(6), 481-494.

Haus, H., Matysek, M., Moßinger, H. and Schlaak, H.F. (2013), "Modelling and characterization of dielectric elastomer stack actuators", *Smart Mater. Struct*., **22**(10), 1-13.

Jager, E., Smela, E. and Inganas, I. (2000), "Microfabricating conjugated polymer actuators", *Science*, **290**, 1540-1545.

John, S.W., Alici, G. and Cook, C.D. (2008), "Validation of resonant frequency model for polypyrrole trilayer actuators", *IEEE/ASME T. Mechatron*., **13**(4), 401-409.

John, S.W., Alici, G. and Cook, C.D. (2010), "Inversion-based feedforward control of polypyrrole trilayer bender actuators", *IEEE/ASME T. Mechatro.*, **15**(1), 149-156.

Kaal, W., Herold, S. and Melz, T. (2010), "Modeling approaches for electroactive polymers", *SPIE Proceedings* San Diego, USA, **7642**, 1-11.

Kaneto, K., Kaneko, M., Min, Y. and MacDiarmid, A.G. (1995), "Artificial muscle: electromechanical actuators using polyaniline films", *Synthetic Metals*, **71**(1-3), 2211-2212.

Kaynak, A., Yang, C., Lim, Y.C. and Kouzani, A. (2011), "Electrochemical fabrication and modelling of mechanical behavior of a tri-layer polymer actuator", *Mater. Chem. Phys*., **125**(1-2), 113-117.
Kaynak, A. (1997), "Effect of synthesis parameters on the surface morphology of polypyrrole thin films", *Mater. Res. Bull*., **32**(3), 271-285.
Madden, D.W. (2000), *Conducting polymer actuators*, PhD Dissertation, MIT, Massachusetts.
Madden, P.G.A. (2003), *Development and modeling of conducting polymer actuators and the fabrication of a conducting polymer based feedback loop*, PhD Dissertation, MIT, Massachusetts.
Madden, J., Vandesteeg, N., Madden, P., Takshi, A., Zimet, R., Anquetil, P., Lafontaine, S., Wierenga, P. and Hunter, I.W. (2004), "Artificial muscle technology: physical principles and naval prospects", *IEEE J. Oceanic Eng*., **29**(3), 706-728.
Mutlu, R., Alici, G. and Li, W. (2013a), "An effective methodology to solve inverse kinematics of electroactive polymer actuators modelled as active and soft robotic structures", *Mech. Machine Theory,* **67**, 94-110.
Mutlu, R., Alici, G. and Li, W. (2013b), "Electroactive polymers as soft robotic actuators: electromechanical modeling and identification", *IEEE/ASME International Conference on Advanced Intelligent Mechatronics (AIM),* Wollongong, Australia, 1096-1101.
Nguyena, C.H., Alici, G. and Wallace, G. (2012), "Modelling trilayer conjugated polymer actuators for their sensorless position control", *Sensor. Actuat. A Phys*., **185**, 82-91.
Otero, T.F. and Teresa Cortes, M. (2001), Characterization of triple layers Smart Structures and Materials: Electroactive Polymer Actuators and Devices; *Proc. SPIE 4329, Smart Structures and Materials: Electroactive Polymer Actuators and Devices*, Newport Beach, CA, USA, July.
Punning, A. (2007), *Electromechanical characterization of ion polymer metal composite sensing actuators*, Ph.D. Dissertation, Tartu University, Tartu, Estonia.
Shahinpoor, M., Kim, J.K. and Mojarrad, M. (2007), *Artificial muscles: applications of Advanced Polymeric Nanocomposites*, CRC Press LLC, Boca Raton, FL, USA.
Shoa, T., Madden, J.D.W., Nigel, R.M. and Yangb, V. (2010), "Analytical modeling of a conducting polymer-driven catheter", *Polymer Int*., **59**(3), 343-351.
Shoa, T., Yoo, D.S., Walus, K. and Madden, J.D.W. (2011), "A dynamic electromechanical model for electrochemically driven conducting polymer actuators", *IEEE/ASME T. Mechatron.*, **16**(1), 42-49.
Smela, E., Inganas, O. and Lundstrom, I. (1995), "Controlled folding of microsize structures", *Science*, **268**, 1735-1738.
Smela, E. (2003), "Conjugated polymer actuators for biomedical applications", *Adv. Mater*., **15**, 481-494.
Torabi, K. and Amiri Moghadam, A.A. (2012), "Robust control of conjugated polymer actuators considering the spatio-temporal dynamics", *J. Syst. Control Eng*., **226**(6), 806-822.
Tso, C.H., Madden, J.D.W. and Michal, C.A. (2007), "An NMR study of PF6− ions in polypyrrole", *Synthetic Metals*, **157**(10-12), 460-466.
Unsworth, J., Lunn, B., Innis, P., Jin, Z., Kaynak, A. and Booth, N. (1992), "Technical review: conducting polymer electronics", *J. Intel. Mat. Syst. Str*., **3**(3), 380-395.
Wallace, G., Spinks, G., Kane-Maguire, L. and Teasdale, P. (2003), *Conductive Electroactive Polymers*, CRC Press LLC, Boca Raton, FL, USA.
Warren, M. (2005), *Electronic and structural effects on the electrochemistry of polypyrrole*, M.Sc. Thesis, University of British Columbia, Vancouver.
Wittbrodt, E., Adamiec-Wójcik, I. and Wojciech, S. (2006), *Dynamics of Flexible Multibody Systems* Springer-Verlag, Berlin Heidelberg, Germany.
Wu, Y., Alici, G., Spinks, G.M. and Wallace, G. (2006), "Fast trilayer polypyrrole bending actuators for high speed applications", *Synthetic Metals*, **156**(16-17), 1017-1022.